16th World Congress in Computational Mechanics (WCCM)
21-26 July 2024, Vancouver, Canada
A. Korobenko, M. Laforest, S. Prudhomme, R. Vaziri (Eds)

NUMERICAL STUDY OF FRACTAL-TREE-GENERATED TURBULENCE

Y. Yin[1], R. Onishi[2], S. Watanabe[3] and I. Segrovets[4]

[1] Faculty of Engineering, Tokyo Institute of Technology
Tokyo 152-8550, JP
yin.y.ae@m.titech.ac.jp

[2] Global Scientific Information and Computing Center, Tokyo Institute of Technology
Tokyo 152-8550, JP

[3] Research Institute for Applied Mechanics, Kyushu University
Fukuoka 816-8580, JP

[4] NABLA Mobility
Tokyo 102-0072, JP

Key words: Turbulence control, Turbulence theory, Wakes, L-system, Fractal tree.

Abstract. We study the aerodynamics of fractal trees by using a simulation based on the Lattice Boltzmann Method with a cumulant collision term. We have applied L-system[1] rules to construct self-similar fractal tree models in aerodynamic computations. We found that the drag coefficient closely matches that of previous literature at high tree-height-based Reynolds numbers ($Re_H \geq 60\,000$). A normalization process capable of collapsing turbulence intensity for various tree models is made. This process reveals that, at the same Reynolds number, different tree models exhibit the same behaviour in the turbulence intensity of their wake region. Our assessment of global and local isotropy in the turbulence generated by fractal trees reveals that the distant wake can be considered nearly locally isotropic at a high Reynolds number ($Re_H \geq 60\,000$). Finally, the present numerical results confirm the non-equilibrium dissipation behaviour previously observed in the case of space-filling fractal square grids[2]. In the wake region, the non-dimensional dissipation rate C_ϵ = constant is not valid. Instead, it is inversely proportional to the local Taylor-microscale-based Reynolds number, $C_\epsilon \propto 1/Re_\lambda$.

1 Introduction

Flow around fractal objects has been widely investigated. In 2007, Hurst & Vassilicos [3] tried 3 major categories and 21 grids and found that the turbulence generated by fractal multi-scale grids showed some unusual properties. After that, most of the research focused on fractal multi-scale grids, and their turbulence was studied both experimentally [2, 4] and numerically [5]. One of the aims of their studies was to generate unexplored turbulent flow conditions at

high Reynolds numbers that differ from the conventional energy dissipation mode $\epsilon \sim k^{3/2}/l$. Here, ϵ represents the energy dissipation rate, k denotes turbulent kinetic energy, and l denotes some local correlation length scale.

In isotropic turbulence, $\epsilon \sim k^{3/2}/l$ becomes $\epsilon = C_\epsilon u^{'3/2}/L$, because in isotropic turbulence $u^{'} = v^{'} = w^{'}$ (where u, v, w are velocity fluctuation in x, y and z-direction, respectively, $^{'}$ represents the root-mean-square (r.m.s.)). Here, C_ϵ denotes a constant non-dimensional dissipation coefficient independent of the Reynolds number, spatial position and time, and L denotes the integral length scale. Seoud & Vassilicos [4] first showed that there is a long wake region of fractal square grids, where the turbulence is approximately isotropic but $C_\epsilon =$ constant does not hold, i.e. the dissipation behaviour is non-equilibrium. Specifically, $C_\epsilon \propto 1/Re_\lambda$, a dissipation anomaly that contradicts classical dissipation theory.

On the other hand, Valente & Vassilicos [6] analyzed turbulence generated by regular grids and found that there is also a long $C_\epsilon \sim 1/Re_\lambda$ non-equilibrium dissipation region in the wake of regular grids. Nagata $et\,al.$ [7] also verified this and found that the turbulence generated by quasi-fractal grids also has an $C_\epsilon \sim 1/Re_\lambda$ non-equilibrium dissipation wake region. This suggests that the $C_\epsilon \sim 1/Re_\lambda$ relationship is not unique to fractal grids, and the non-equilibrium dissipation phenomena are likely to be widespread in various turbulent flows. It is possibly not limited to 2D fractal grid planes but also applies to 3D fractal objects, such as trees.

Trees, as a very common object in real life, have a good blocking effect on airflow (shelter effect) due to their large size and fractal shape, so most of the studies on trees have focused on calculating the drag coefficient and aerodynamic porosity[8, 9, 10, 11, 12]. However, the studies focused on the dissipation behaviour of the wake region are limited. In this paper, we investigate the turbulence generated by fractal trees under high Reynolds number conditions using quasi-DNS simulations based on a cumulant Lattice Boltzmann Method (LBM) [13] on multi-GPU parallelization. The Adaptive Mesh Refinement (AMR) method is also introduced.

2 Numerical method

2.1 Lattice Boltzmann Method (LBM)

A code based on the Lattice Boltzmann Method (LBM) with a cumulant collision term is employed for our numerical computations. LBM treats the fluid as a collection of virtual particles and computes the evolution of their velocity distribution function over time. To accurately simulate flows at high Reynolds numbers, the D3Q27 Cumulant collision model [13] is utilized. This model has high numerical stability and computational accuracy. LBM is fully explicit and does not involve iterative calculations such as the Poisson equation for pressure in the conventional difference method, thus achieving high computational performance in large-scale calculations.

2.2 Adaptive Mesh Refinement (AMR)

A high-resolution grid is necessary to accurately resolve a fractal tree's boundary layer and wake region. However, employing a uniform high-resolution grid throughout the entire computational domain would lead to an enormous number of grid points, requiring impractical

amounts of computational resources. To maintain accuracy and reduce computational costs, an Adaptive Mesh Refinement method (AMR method) is utilized. By recursively subdividing the computational grids, high-resolution grids can be allocated to arbitrary regions [14]. The finest grids near the tree surface and somewhat finer grids in the wake region are allocated. In other distant locations, coarse grids are assigned. More details about the AMR-LBM can be found in the previous paper [15].

2.3 Interpolated bounce-back method

The Lattice Boltzmann Method utilizes orthogonal grids for computation. For object shapes that do not conform to grid directions, like the surface of a fractal tree, we avoid the traditional stair-stepped representation of object shapes. Instead, a second-order accurate Interpolated bounce-back method [16] is introduced to establish boundary conditions. By employing the D3Q27 type of Lattice Boltzmann Method, the object's surface can be precisely represented in 26 directions. This capability substantially enhances the accuracy of our model. The fluid forces acting on the object surface are calculated based on the momentum exchange [17] between the velocity distribution function and the object at the object boundary.

2.4 Fractal tree model

This paper chooses a unique algorithm called the L-system [1] to produce fractal tree representations. The algorithm of the parametric L-system is shown in the following equation. The first line of (1) represents the parameters of the central trunk part of a tree. The second and subsequent lines represent branch generation rules. More details about the parametric L-system can be found in the previous paper [1].

$$\begin{aligned} &\omega : A(100, w_0) \\ &p_1 : A(s, w) : s \geq min \ \rightarrow !(w)F(s) \\ &\quad [+(\alpha_1)/(\varphi_1)A(s * r_1, w * q^e)] \\ &\quad [+(\alpha_2)/(\varphi_2)A(s * r_2, w * (1-q)^e)] \end{aligned} \tag{1}$$

For the present work, using the parameters stated in Table 1, three kinds of fractal tree geometries are generated using the parametric L-system. Then, all three kinds of tree heights (H) are normalized to 1 metre while keeping the horizontal and vertical scales the same; see figure 1. Table 2 summarizes the various tree geometries used in this study.

2.5 Simulation setup

The computation domain is $32H \times 16H \times 16H$. The tree's centre of mass is calculated and placed at $(8H, 8H, 8H)$ as shown in figure 2, and uniform flow in the x-direction for inflow conditions. Trees are treated as rigid bodies, and deformation due to fluids is not considered. Using physical properties of air at room temperature, density $\rho = 1.205\,\mathrm{kg/m^3}$, kinematic viscosity $\nu = 1.512 \times 10^{-5}\,\mathrm{m^2/s}$.

Model name	r_1	r_2	α_1	α_2	φ_1	φ_2	ω_0	q	e	min	n
Basic n = 4	0.8	0.8	30	-30	137	137	30	0.5	0.5	0.02	4
Basic n = 6	0.8	0.8	30	-30	137	137	30	0.5	0.5	0.02	6
Basic n = 8	0.8	0.8	30	-30	137	137	30	0.5	0.5	0.02	8

Table 1: Parameters for fractal trees shown in figure 1 using equation 1.

Model	Basic n = 4	Basic n = 6	Basic n = 8
D_0/H	107.15	86.64	77.16
L_0/H	357.35	288.94	257.32

Table 2: Fractal trees geometry details.

After evaluating the resolution dependency of the drag coefficient (C_D), for basic n = 4, 6, 8, the finest grid $\Delta x/H = 1/1024$, $1/1024$ and $\Delta x/H = 1/2048$ are placed near the surface of the tree (about 40 meshes from the surface), respectively. For all three tree models, $\Delta x/H = 1/512$ grids are placed in the wake region with a length of about $8.0H$. We confirmed that for three tree models, at Re_H = 120 000, the mesh resolution in the wake region is $\Delta x \approx 2.0\eta$, where η denotes Kolmogorov scale. Figure 3 shows an example of AMR grids in the case of basic n = 8. The total grid numbers are 1 682 158 592, 1 711 257 088, and 2 363 039 744 in the case of basic n = 4, n = 6 and n = 8, respectively. An outflow boundary condition is imposed on the calculation boundary behind the tree, and an inflow boundary condition is imposed on the other calculation boundaries. The calculations were performed on the TSUBAME 4.0 supercomputer at Tokyo Institute of Technology. For basic n = 4 and n = 6, 12 GPUs of NVIDIA H100 were utilized. It took approximately 48 and 54 hours to calculate a non-dimensional time of 60 for n = 4 and n = 6, respectively. In the case of basic n = 8, 16 GPUs of NVIDIA H100 were utilized and were completed within 72 hours to calculate a non-dimensional time of 60. Here, the non-dimensional time is defined as Ut/H, U is the uniform flow velocity, t is the physical time, and H is the tree's height. As shown in table 3, calculations were carried out for four cases with different tree height-based Reynolds numbers Re_H.

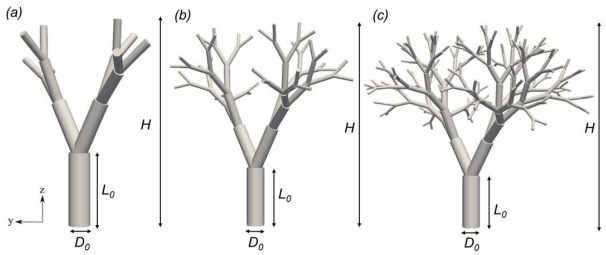

Figure 1: Side view of the fractal tree geometry for (a) basic n = 4; (b) basic n = 6; and (c) basic n = 8. Axis conventions are the same as that used in the simulation.

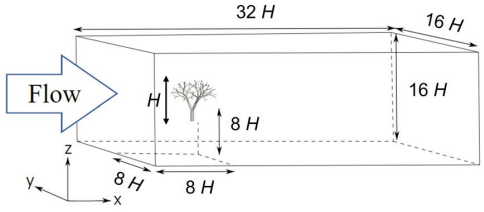

Figure 2: Computational domain and arrangement of trees.

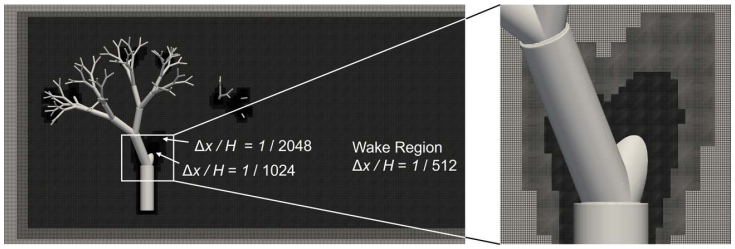

Figure 3: Computational grid subdivided hierarchically around basic n = 8 tree.

3 Results

3.1 Comparison of drag coefficient to literature

Figure 4 shows the relationship between Re_H and C_D. Grant & Nickling [8] designed a direct field measurement and showed a decrease in C_D values with increasing Reynolds number at $Re_H = 15\,000$ and 25 000. The simulations of this study qualitatively reproduced the decrease in CD values with increasing Re_H. Manickathan $et\,al.$ [12] showed that the C_D values keep almost the same when $Re_H \geq 60\,000$ whatever model trees or natural trees by using wind tunnel measurement. Gillies $et\,al.$ [9] also used wind tunnel and showed that the C_D values keep almost the same when $Re_H \geq 200\,000$ in the case of Burning Bush and Colorado Spruce, the tree with branches. In this study, all three tree models showed a tendency for C_D to decrease with increasing Reynolds number at low and medium Reynolds number (Re_H = 2500 to 10 000). However, after Re_H exceeded 60 000, C_D remained almost constant. This is in qualitative agreement with the study by Grant & Nickling [8] and Manickathan $et\,al.$ [12], despite our tree model not including leaves.

3.2 Turbulence intensity

Turbulence intensity is defined by the following equation. Here, u'_{avg} is the average of $\overline{u_i^2}$ in 3 directions and u_i is the velocity fluctuation in i direction.

$$\frac{u'_{avg}}{U} = \frac{\sqrt{\frac{1}{3}\sum_i \overline{u_i^2}}}{U} \tag{2}$$

In previous research of fractal-grid-generated turbulence, Gomes-Fernandes $et\,al.$ [2] de-

$Case$	$U(\mathrm{m/s})$	Re_H
A	0.0378	2500
B	0.1512	10 000
C	0.9072	60 000
D	1.8144	120 000

Table 3: Uniform flow velocity and Re_H for the four simulation cases.

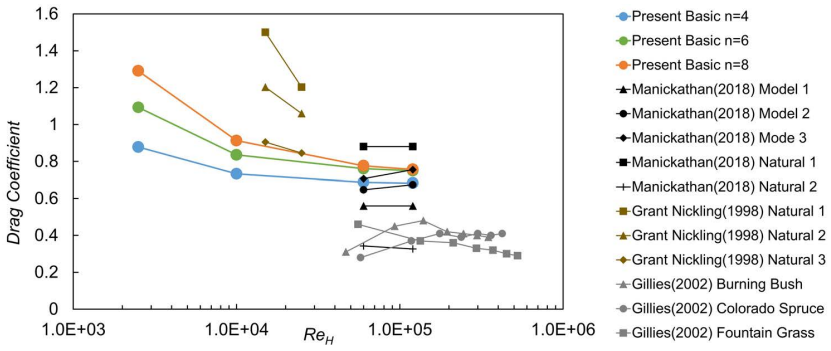

Figure 4: Relationship between C_D and Re_H obtained in this study and comparison with previous studies.

fined a method to normalize centreline turbulence intensity. This method is also used in the present study, where normalization is performed by dividing the turbulence intensity by its peak value and then dividing x by the x-coordinate where the turbulence intensity is maximum (x_{peak}). Figure 5 shows the result using this normalization. It can be seen that the turbulence intensity collapses better when the Reynolds number is high, and except for the case of basic n = 4, the turbulence intensity of n = 6 and n = 8 collapses very well. It is considered that the generation, development and decay of turbulence intensity are qualitatively the same regardless of the tree shape after a critical fractal iteration number (n) is reached (e.g. $n \geq 6$).

3.3 Global and local isotropy

In this section, the isotropy of the wake region of fractal trees is assessed. For clarity, we only show the basic n = 8 data. Note that all the other models also show very similar values and the same trend. Figure 6 shows a comparison of centreline global isotropy parameters $u^{'}/v^{'}$, $u^{'}/w^{'}$ and $v^{'}/w^{'}$ at various Reynolds numbers for basic n = 8. It can be seen that at high Reynolds numbers, all three parameters generally hover around 1.0 and slightly smaller than 1.2, indicating that the flow is globally isotropic if $x/x_{peak} \geq 1.0$.

The local isotropy is assessed using two relations (K_1, K_3) derived by Taylor [18] as shown in equation 3. Figure 7 compares centreline local isotropy parameters K_1, K_3 at various Reynolds numbers for basic n = 8. Similar to global isotropy parameters, it can be seen that at high Reynolds numbers, K_1 and K_3 generally hover around 1.0, close to previous grid turbulence study [2]. In conjunction with the previously described, the wake region for $x/x_{peak} > 1.0$ can

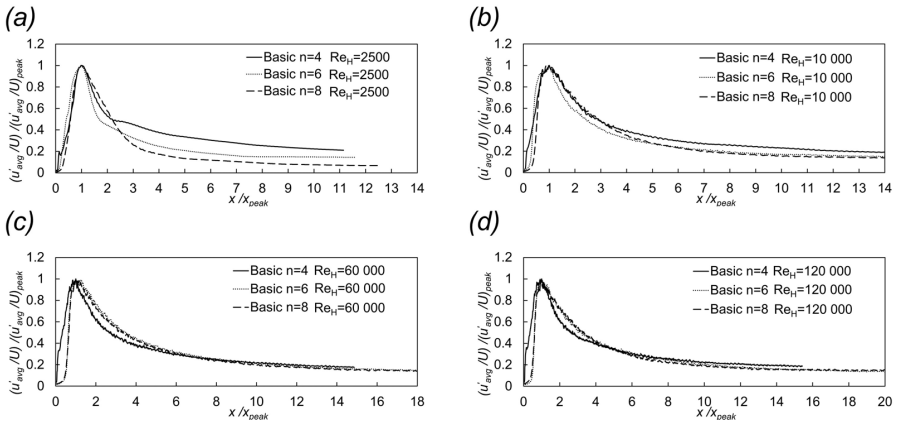

Figure 5: Streamwise evolution of centreline turbulence intensity normalized by its peak value is given as a function of x/x_{peak} at (a) $Re_H = 2500$, (b) $Re_H = 10\,000$, (c) $Re_H = 60\,000$ and (d) $Re_H = 120\,000$.

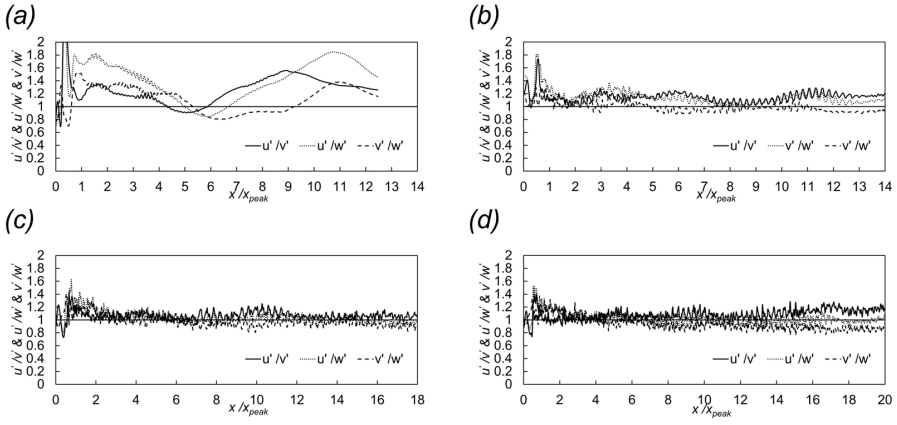

Figure 6: Global isotropy parameters of centreline for basic n = 8 at (a) $Re_H = 2500$, (b) $Re_H = 10\,000$, (c) $Re_H = 60\,000$ and (d) $Re_H = 120\,000$.

be regarded as associate isotropic at high Reynolds numbers.

$$K_1 = 2\,\overline{(\frac{\partial u}{\partial x})^2}/\overline{(\frac{\partial v}{\partial x})^2}, \quad K_3 = 2\,\overline{(\frac{\partial u}{\partial x})^2}/\overline{(\frac{\partial u}{\partial y})^2} \tag{3}$$

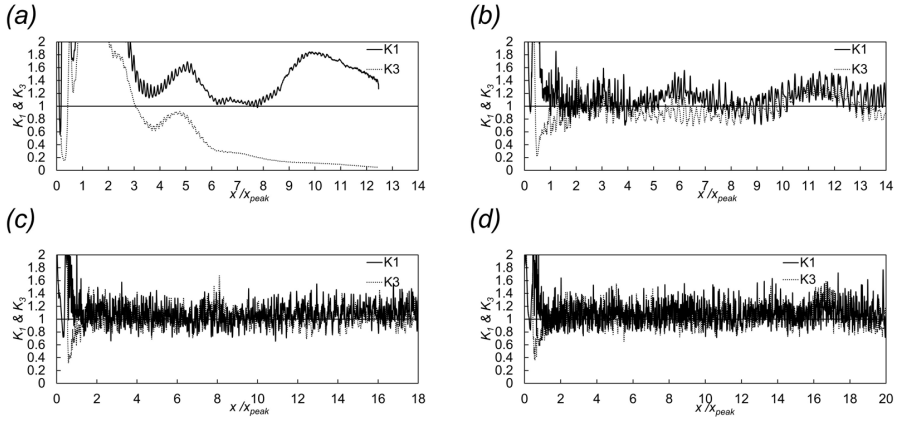

Figure 7: Local isotropy parameters of centreline for basic n = 8 at (a) $Re_H = 2500$, (b) $Re_H = 10\,000$, (c) $Re_H = 60\,000$ and (d) $Re_H = 120\,000$.

3.4 Dissipation and non-equilibrium nature

This section examines dissipation and non-equilibrium characteristics in the decay region. Specifically, the integral length scale L and non-dimensional dissipation rate C_ϵ are investigated. There is a "cornerstone dissipation scaling of turbulence theory" that the energy dissipation rate can be scaled as the following equation when the Reynolds number is high enough [19].

$$\epsilon = C_\epsilon \frac{u^{'3}}{L} \tag{4}$$

Here, C_ϵ is a constant. When the Reynolds number is high enough, the flow in the wake region can be regarded as locally isotropic, and $\epsilon = 15\nu\frac{u^{'2}}{\lambda^2}$ can express the energy dissipation rate. Also, considering Taylor microscale $\lambda = \sqrt{\overline{u^2}/\overline{(\partial u/\partial x)^2}}$ and local Taylor Reynolds number $Re_\lambda = u^{'}\lambda/\nu$, the relation $\frac{L}{\lambda} \propto Re_\lambda$ can be derived. This relation holds when C_ϵ is a constant, and the wake region is locally isotropic. Estimating the integral length scale is necessary to verify if the present study follows this relation. The integral length scale is estimated by calculating the longitudinal correlation function $f(r,x) = \overline{u(x)u(x+r)}/\overline{u(x)^2}$. If $L_u/\lambda \propto Re_\lambda$ holds true, then equation 4 holds true with a constant C_ϵ. Conversely, then C_ϵ is not a constant value but $C_\epsilon \propto 1/Re_\lambda$, varies with position in the wake region.

Figure 8 (a) and (b) show the variation of L_u/λ in the streamwise distance as a function of x/x_{peak} and Re_λ. As can be seen from the figure, in the decaying region of $x \geq x_{peak}$, in which

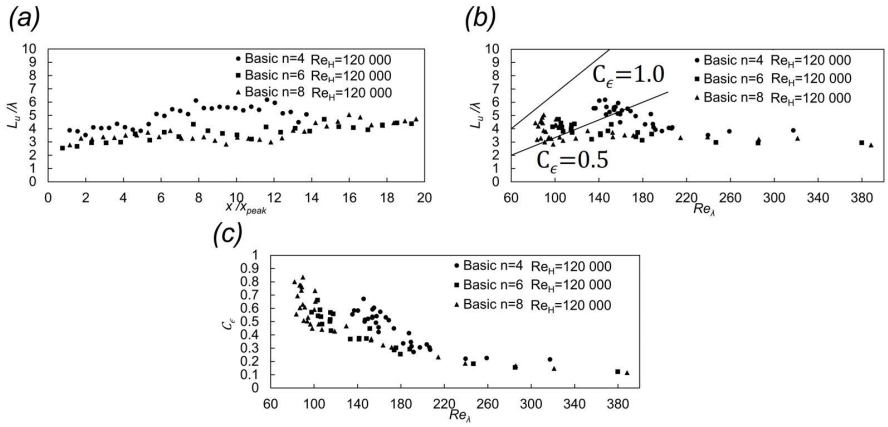

Figure 8: Integral length scale to Taylor microscale ratio L_u/λ for different tree models in relation to (a) x/x_{peak}, (b) Re_λ and (c) non-dimensional energy dissipation rate parameter C_ϵ in relation to Re_λ.

Re_λ decreases, L_u/λ for all three models does not show a significant decrease. It is suggested that 4 does not apply to the flow in the decaying region of the fractal-tree-generated turbulent flow. Figure 8 (c) shows the variation of C_ϵ as a function of Re_λ. It can be seen that C_ϵ is inversely proportional to Re_λ, which achieves qualitative agreement with results from previous studies of fractal-grid-generated turbulence [2, 4].

4 Conclusions

This study successfully employed large-scale numerical simulations for the fluid around fractal trees using AMR-LBM. The main contribution of this paper is the elucidation of the dependence of the drag coefficient of trees on tree shape and Reynolds number, as well as the non-equilibrium dissipation behaviour $C_\epsilon \propto 1/Re_\lambda$ in the wake region of fractal trees, which is consistent with the non-equilibrium decay turbulence observed in fractal grids [2, 4]. Moreover, various turbulence statistics and scales, including turbulence intensity, global and local isotropy parameters, were also presented.

Three kinds of tree models with fractal iteration numbers n = 4, 6, 8 were generated through the parametric L-system. At low and medium Reynolds numbers, the drag coefficient increases with the fractal iteration numbers n and decreases with the Reynolds number. However, at high Reynolds numbers (Re_H = 120 000), if the fractal iteration number is greater than a certain value ($n \geq 6$), the drag coefficient becomes independent of fractal iteration number n and Reynolds number and tends to a constant value.

Energy dissipation scaling was investigated, and it was confirmed that at high Reynolds number ($Re_H = 120\,000$), the integral length scale to Taylor microscale ratio L_u/λ remains approximately constant while Taylor microscale-based Reynolds number Re_λ decreases in the wake region of $x/x_{peak} \geq 1$. Consequently, the energy dissipation in the fractal tree wake region does not follow the conventional scaling $\epsilon = C_\epsilon \frac{u'^3}{L}$, since C_ϵ is not a constant, but $C_\epsilon \propto 1/Re_\lambda$, which is consistent with the non-equilibrium dissipation behaviour reported in the wake region

of 2D fractal grids.

In terms of other turbulence statistics, it was found that the wake interaction length scale x_{peak} introduced by [2] can also be employed to normalize the centreline turbulence intensity in the wake region of fractal trees. At high Reynolds numbers (e.g. $Re_H \geq 60\,000$), this normalization method can collapse the turbulence intensity of fractal trees with different shapes if the fractal iteration number reaches a certain threshold (e.g. $n = 6$). Furthermore, the isotropy characteristics were investigated. At high Reynolds numbers ($Re_H \geq 60\,000$), it was found that the wake region of fractal trees can be considered essentially isotropic.

Acknowledgements

This work is supported by "Joint Usage/Research Center for Interdisciplinary Large-scale Information Infrastructures (JHPCN)" in Japan (Project ID: jh240041). This work was also supported by JST SPRING, Japan Grant Number JPMJSP2106.

REFERENCES

[1] P. Prusinkiewicz, M. Hammel, J. Hanan, and R. Mech. L-systems: from the theory to visual models of plants. In *Proceedings of the 2nd CSIRO Symposium on Computational Challenges in Life Sciences*, volume 3, pages 1–32. Citeseer, 1996.

[2] R. Gomes-Fernandes, B. Ganapathisubramani, and J. C. Vassilicos. Particle image velocimetry study of fractal-generated turbulence. *Journal of Fluid Mechanics*, 711:306–336, 2012.

[3] D. Hurst and J. C. Vassilicos. Scalings and decay of fractal-generated turbulence. *Physics of Fluids*, 19(3):035103, 2007.

[4] R. E. Seoud and J. C. Vassilicos. Dissipation and decay of fractal-generated turbulence. *Physics of fluids*, 19(10):105108, 2007.

[5] K. Nagata, H. Suzuki, Y. Sakai, T. Hayase, and T. Kubo. Direct numerical simulation of turbulence characteristics generated by fractal grids. *Int. Rev. Phys*, 2(6):400, 2008.

[6] P. Valente and J. C. Vassilicos. Universal dissipation scaling for nonequilibrium turbulence. *Physical review letters*, 108(21):214503, 2012.

[7] K. Nagata, T. Saiki, Y. Sakai, Y. Ito, and K. Iwano. Effects of grid geometry on non-equilibrium dissipation in grid turbulence. *Physics of Fluids*, 29(1):015102, 2017.

[8] P. F. Grant and W. G. Nickling. Direct field measurement of wind drag on vegetation for application to windbreak design and modelling. *Land Degradation & Development*, 9(1):57–66, 1998.

[9] J. A. Gillies, W. G. Nickling, and J. King. Drag coefficient and plant form response to wind speed in three plant species: Burning bush (euonymus alatus), colorado blue spruce (picea pungens glauca.), and fountain grass (pennisetum setaceum). *Journal of Geophysical Research: Atmospheres*, 107(D24):ACL–10, 2002.

[10] D. Guan, Y. Zhang, and T. Zhu. A wind-tunnel study of windbreak drag. *Agricultural and forest meteorology*, 118(1-2):75–84, 2003.

[11] J. P. Bitog, I.-B. Lee, H.-S. Hwang, M.-H. Shin, S.-W. Hong, I.-H. Seo, E. Mostafa, and Z. Pang. A wind tunnel study on aerodynamic porosity and windbreak drag. *Forest Science and technology*, 7(1):8–16, 2011.

[12] L. Manickathan, T. Defraeye, J. Allegrini, D. Derome, and J. Carmeliet. Comparative study of flow field and drag coefficient of model and small natural trees in a wind tunnel. *Urban forestry & urban greening*, 35:230–239, 2018.

[13] M. Geier, M. Schönherr, A. Pasquali, and M. Krafczyk. The cumulant lattice boltzmann equation in three dimensions: Theory and validation. *Computers & Mathematics with Applications*, 70(4):507–547, 2015.

[14] M. Wahib, N. Maruyama, and T. Aoki. Daino: a high-level framework for parallel and efficient AMR on GPUs. In *SC'16: Proceedings of the International Conference for High Performance Computing, Networking, Storage and Analysis*, pages 621–632. IEEE, 2016.

[15] S. Watanabe and T. Aoki. Large-scale flow simulations using lattice Boltzmann method with AMR following free-surface on multiple GPUs. *Computer Physics Communications*, 264:107871, 2021.

[16] M. Bouzidi, M. Firdaouss, and P. Lallemand. Momentum transfer of a boltzmann-lattice fluid with boundaries. *Physics of fluids*, 13(11):3452–3459, 2001.

[17] B. Wen, C. Zhang, Y. Tu, C. Wang, and H. Fang. Galilean invariant fluid–solid interfacial dynamics in lattice boltzmann simulations. *Journal of Computational Physics*, 266:161–170, 2014.

[18] G. I. Taylor. Statistical theory of turbulenc. *Proceedings of the Royal Society of London. Series A-Mathematical and Physical Sciences*, 151(873):421–444, 1935.

[19] H. Tennekes and J. L. Lumley. *A first course in turbulence*. MIT press, 1972.